Molecular Therapy
Methods & Clinical Development
Original Article

CRISPR-Cas9-mediated genome editing delivered by a single AAV9 vector inhibits HSV-1 reactivation in a latent rabbit keratitis model

Nadia Amrani,[1,4] Kevin Luk,[1,4] Pankaj Singh,[2] Mason Shipley,[2] Meltem Isik,[1] Martina Donadoni,[3] Anna Bellizzi,[3] Kamel Khalili,[3] Ilker K. Sariyer,[3] Donna Neumann,[2] Jennifer Gordon,[1] and Guo-Xiang Ruan[1]

[1]Excision BioTherapeutics Inc, Watertown, MA, USA; [2]Department of Ophthalmology and Visual Sciences, University of Wisconsin-Madison, Madison, WI, USA; [3]Center for Neurovirology and Gene Editing, Department of Microbiology, Immunology and Inflammation, Temple University Lewis Katz School of Medicine, Philadelphia, PA, USA

Herpes simples virus 1 (HSV-1) keratitis is a major cause of blindness globally. During primary infection, HSV-1 travels to the trigeminal ganglia and establishes lifelong latency. Although some treatments can reduce symptom severity and recurrence, there is no cure for HSV-1 keratitis. We used CRISPR-Cas9 to co-target gene sequences encoding two essential HSV-1 proteins, ICP0 and ICP27, as a potential therapy for HSV-1 keratitis. In HSV-1-infected Vero cells, the HSV-1 viral load and titer were significantly reduced by plasmid transfection or AAV2 vector transduction expressing Cas9 nuclease from *Staphylococcus aureus* (SaCas9) and paired guide RNAs (gRNAs). Off-target assessment showed minimal off-target editing activity from the selected gRNAs. We then tested our CRISPR-Cas9 gene editing approach in a latent rabbit model of HSV-1 keratitis. Corneal scarification with all-in-one AAV8(Y733F)-SaCas9 or AAV9-SaCas9 vector reduced viral shedding by over 50%. Interestingly, intravenous administration of the same AAV9-SaCas9 vector eliminated viral shedding in 92% of treated eyes. In addition, treated trigeminal ganglia showed a reduction in HSV-1 DNA and RNA expression. Our results support the utility of single-dose AAV9 all-in-one CRISPR-Cas9 gene editing as a safe and effective strategy for treating HSV-1 keratitis.

INTRODUCTION

Herpes simplex virus 1 (HSV-1) is one of the most common human viruses affecting approximately 3.7 billion individuals under the age of 50 (67%) worldwide.[1] It is the most frequent cause of infectious blindness in the developed world.[2] HSV-1 is a neurotropic virus that first enters the axons of sensory neurons then migrates to the trigeminal ganglia (TG) and other ganglia tissues, where it persists in a latent state. Periodically, reactivated HSV-1 travels back along the axons to the cornea, causing recurrent herpes keratitis.[3] Herpes keratitis manifestations include corneal opacity, edema, corneal scarring, and neovascularization, which can lead to irreversible vision impairment and blindness.[4]

Currently, there is no vaccine to prevent HSV-1 infection or therapies to eliminate the virus from latent reservoirs. HSV-1 can evade the immune antiviral defenses and establish lifelong latency. The standard of care involves using nucleoside analogs such as acyclovir, ganciclovir, trifluridine, and vidarabine that inhibit HSV polymerase or thymidine kinase during viral replication.[5] These treatments reduce the severity of acute infections, and the frequency of recurrent infections. However, they cannot eliminate the latent HSV-1 reservoirs, and their prolonged use can lead to the emergence of resistant HSV-1 strains, especially in immunocompromised patients.[6,7]

Genome editing tools such as meganuclease and clustered regularly interspaced short palindromic repeats (CRISPR)/CRISPR-associated protein 9 (Cas9) system have been used to target a variety of genetic and infectious diseases, including HSV-1 keratitis.[8–10] The meganuclease-based therapeutic approach inhibited HSV-1 replication, disrupted latent HSV-1 reservoirs in the mouse model, and led to a reduction in viral reactivation.[11,12] Recently, Wei and colleagues employed a combinatorial therapeutic approach, using CRISPR-Cas9-mediated gene editing alongside corneal transplantation, to treat patients with herpes keratitis in a clinical trial.[13,14] The Cas9-coding mRNA and the guide RNAs were delivered in lentiviral particles directly into the graft bed of the eye that received a new corneal transplantation. The three patients treated in this study were free of viral relapse at 18-months post-treatment. However, safety risks exist with the use of lentiviral vectors, which may integrate into the host genome randomly. In addition, it is unclear how much of the observed benefit in reduction of viral shedding was contributed by the simultaneous corneal transplantation.

Previous studies indicated that using a single guide RNA (gRNA) to eliminate HIV-1 led to the creation of escape mutants.[15–18] Use of a

Received 1 May 2024; accepted 18 July 2024;
https://doi.org/10.1016/j.omtm.2024.101303.

[4]These authors contributed equally

Correspondence: Donna Neumann, Department of Ophthalmology and Visual Sciences, University of Wisconsin-Madison, 677A Medical Sciences Center, 1300 University Avenue, Madison, WI 53706, USA.
E-mail: dneumann3@wisc.edu
Correspondence: Guo-Xiang Ruan, Excision BioTherapeutics Inc, 134 Coolidge Avenue, Watertown, MA 02472, USA.
E-mail: eruan@excisionbio.com

Table 1. Spacer and target sequences of the SaCas9 gRNAs targeting *ICP0* and *ICP27*

Guide name	Spacer sequence	Target sequence with PAM and flanking sequences (in lower case)
ICP0g1	GUACCCGACGGCCCCCGCGU	cccgaGTACCCGACGGCCCCCGCGTCGGAGTggaac
ICP0g2	CUCAGGCCGCGAACCAAGAA	cctggCTCAGGCCGCGAACCAAGAACAGAGTctgtg
ICP27g1	AAUCCUAGACACGCACCGCC	atcgaAATCCTAGACACGCACCGCCAGGAGTgttcg
ICP27g2	UCGCCAGCGUCAUUAGCGGG	ggcaaTCGCCAGCGTCATTAGCGGGGGGGGTgcttg

single gRNA to disrupt the HSV-1 genome may lead to a similar phenomenon after DNA repair. Therefore, simultaneously targeting two or more viral sites, which can induce large DNA deletions, can more effectively prevent viral replication and avoid virus survival. To test this hypothesis, we delivered Cas9 nuclease from *Staphylococcus aureus* (SaCas9) and two chimeric gRNAs targeting two immediately early genes in HSV-1, *ICP0* and *ICP27*, with an all-in-one (AIO) adeno-associated virus (AAV) vector, as a potential therapeutic approach to treat latent HSV-1 keratitis.

ICP0 and ICP27 proteins regulate the expression of multiple early and late genes.[19,20] Furthermore, during latency, most of the HSV-1 genome is in a silenced heterochromatin state. Conversely, the transcriptionally active locus of *latency-associated transcript* (*LAT*) displays markers of open chromatin.[21] It is known that chromatin modifications to the genomes can significantly impact the efficacy of gene editing.[22] *ICP0* overlaps with *LAT* locus, and *ICP27* is in an adjacent region as well. The accessibility of these two genes could be important in the efficacy of targeting latent HSV-1 for gene editing. Last, *ICP0* is duplicated in the HSV-1 genome.[19,20] Therefore, using two gRNAs co-targeting *ICP0* and *ICP27* may potentially introduce three double-stranded DNA breaks in the latent HSV-1 genome. This could result in various deletions within the HSV-1 viral genome, effectively preventing viral replication and escape following DNA repair.

We showed that the AIO AAV vector expressing SaCas9 and paired gRNAs nearly eliminated the viral load and viral titer in HSV-1-infected Vero cells. *In vivo*, we observed over 50% reduction in viral shedding in the treated eyes of a latent rabbit model of HSV-1 keratitis when the vectors were delivered by corneal scarification, and complete inhibition of viral shedding in 11 out of 12 treated eyes when the vectors were delivered by intravenous (i.v.) administration. Moreover, we observed reduced HSV-1 viral DNA and *LAT* RNA in the TG of treated rabbits. Therefore, our therapeutic gene editing approach could effectively target the latent HSV-1 reservoirs in the rabbit HSV-1 keratitis model. Together, these results suggest that our therapeutic payload may potentially serve as a one-time curative therapy for patients who are affected by HSV-1 keratitis.

RESULTS

Efficient editing of HSV-1 genes in HEK293FT stable cell line using SaCas9 and paired gRNAs

To design conserved gRNAs targeting *ICP0* and *ICP27*, we first built an HSV-1 genome database using the Virus Pathogen Resource (ViPR) database (Version Feb, 2022; 46,027 HSV-1 strains and 62,554 GenBank IDs) and generated consensus coding sequences for *ICP0* and *ICP27* (Figures S1A and S1B). Two SaCas9 gRNAs targeting *ICP0* and two SaCas9 gRNAs targeting *ICP27* (Table 1) were selected based on sequence match to HSV-1 strains in our curated database (>70%) and number of *in silico* nominated off-target sites (Table 2).[23] The locations of these four SaCas9 gRNAs in the HSV-1 genome are shown in Figure S2A.

Next, we evaluated the activity of these four guides complexed with SaCas9 in our HEK293FT stable reporter cell line, which has the consensus coding sequences of *ICP0* and *ICP27* inserted in the *AAVS1* locus (Figure S2B and materials and methods). We demonstrated that co-transfection with two plasmids expressing each gRNA induced efficient DNA excisions between the two target sites (Figure S2C). These results demonstrated that SaCas9/gRNA can induce efficient excision of the HSV-1 DNA in our reporter cell line.

SaCas9/gRNAs efficiently reduced HSV-1 viral load and titer in Vero cells

We next evaluated the efficacy of our SaCas9/gRNA multiplex strategy in reducing HSV-1 load and titer by transfecting Vero cells, which are derived from the kidney of an African green monkey, with six combinations of gRNA pairs consisting of the four gRNAs targeting *ICP0* and *ICP27*. Briefly, Vero cells were co-transfected with two

Table 2. Number of *in silico* nominated off-target sites in the human genome for the four SaCas9 gRNAs

Number of mismatches	0	1		2		3		4	5	
Number of bulges	1	0	1	0	1	0	1	0	0	Total
ICP0g1	0	0	0	0	1	1	44	18	294	**358**
ICP0g2	0	0	0	0	8	5	190	50	657	**910**
ICP27g1	0	0	0	0	2	1	122	23	295	**443**
ICP27g2	0	0	1	0	5	1	68	20	221	**316**

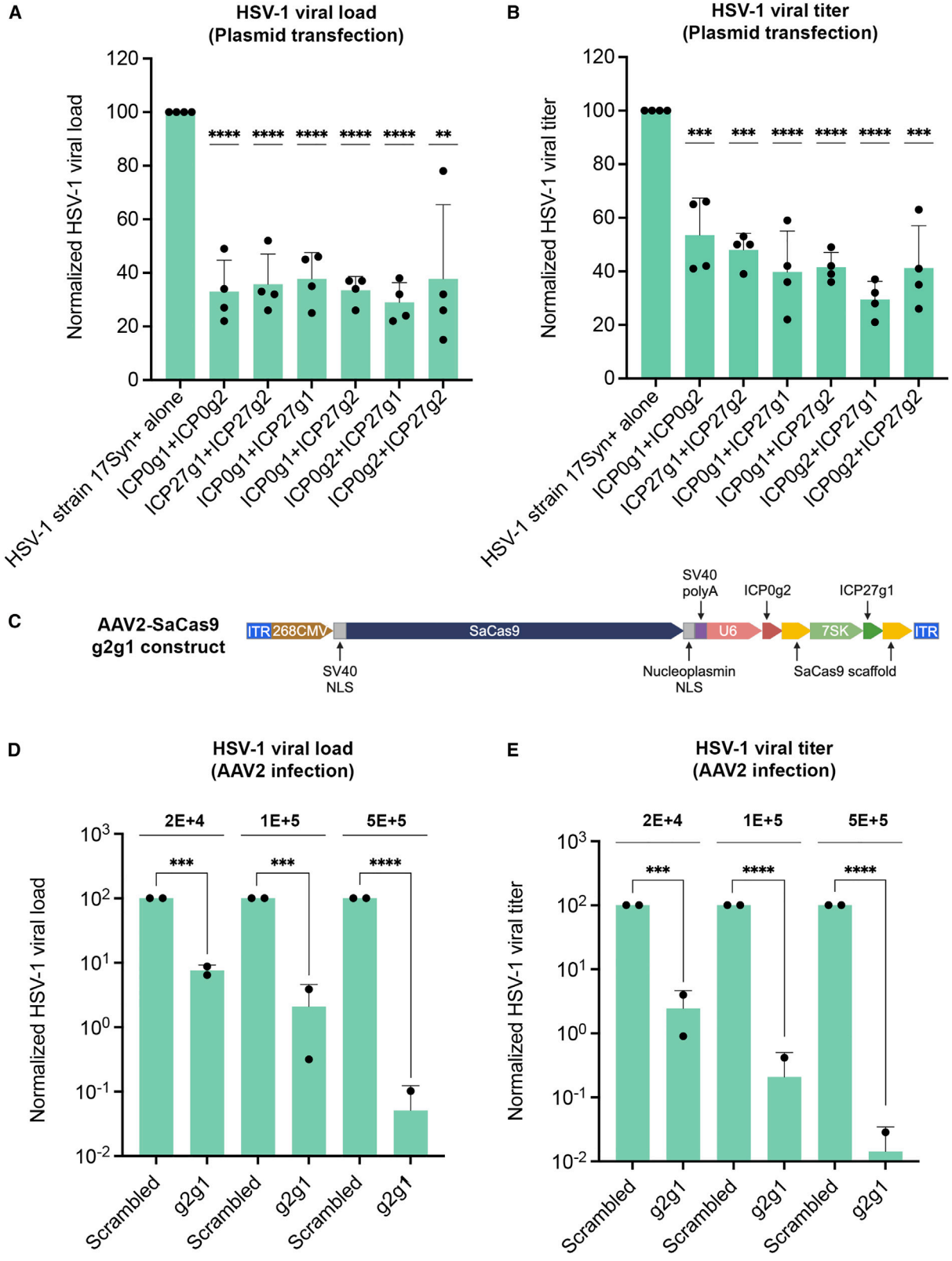

(legend on next page)

plasmids, both expressing SaCas9 nuclease and each individual gRNA, and then infected with HSV-1 17Syn+ virus for 3 h at a multiplicity of infection (MOI) of 5E−4 plaque-forming units (pfu) per cell. At 48 h post-infection, the cells were collected for viral DNA quantification and the supernatants were collected for measuring the abundance of infectious viral particles (viral titer). Droplet digital PCR (ddPCR) analysis revealed that Vero cells transfected with the six different combinations of gRNA pairs resulted in the reduction of HSV-1 viral load by 62%–71%, compared with the untreated HSV-1 infected cells (Figure 1A). To determine the impact of CRISPR-Cas9-mediated gene editing on the generation of HSV-1 progeny, we assessed the viral titer present in the supernatants by plaque assay. As expected, we observed a significant reduction in the HSV-1 viral titer in the treated Vero cells by 47%–71% compared with the untreated cells (Figure 1B). Both ddPCR and plaque assays showed that the ICP0g2/ICP27g1 pair, hereinafter referred to as SaCas9-g2g1, led to the greatest inhibition of HSV-1. Taken together, these results demonstrated that simultaneous targeting of multiple HSV-1 sites with CRISPR-Cas9 can efficiently reduce the viral load and titer in infected Vero cells.

Since the SaCas9-g2g1 pair demonstrated the greatest efficacy when co-delivered as two plasmids to HSV-1-infected Vero cells, this gRNA pair was selected for further characterization. We constructed an AIO AAV plasmid expressing SaCas9 and both ICP0g2 and ICP27g1 gRNAs (Figure 1C). We first produced AAV2 vector to test the efficiency of SaCas9-g2g1 in Vero cells, since the AAV2 serotype can efficiently transduce Vero cells. The Vero cells were transduced with either the AAV2-SaCas9 scrambled vector (non-targeting gRNA control) or with the AAV2-SaCas9-g2g1 vector at an MOI of 2E+4, 1E+5, or 5E+5 vector genomes (vg)/cell for 48 h. The cells were then infected with HSV-1 17Syn+ virus at an MOI of 5E−4 pfu/cell for 3 h. Forty-eight hours later, the impact of the AAV2 vector on HSV-1 replication was assessed by ddPCR and plaque assay. Compared with the scrambled vector control, the AAV2-SaCas9-g2g1 vector significantly reduced the HSV-1 viral load and infectious titer in a dose-dependent manner. Specifically, at an MOI of 2E+4, 1E+5, and 5E+5 vg/cell, the AAV2-SaCas9-g2g1 vector reduced the HSV-1 viral load by 92.39%, 97.92%, and 99.95%, respectively (Figure 1D), and decreased the HSV-1 viral titer by 97.55%, 99.79%, and 99.99%, respectively (Figure 1E). Our data showed that SaCas9-g2g1 can substantially inactivate and reduce the HSV-1 virus in infected cells and suggested that this pair could be a potential treatment for HSV-1 infection *in vivo*.

Off-target assessment of ICP0g2 and ICP27g1

Although we demonstrated that SaCas9-g2g1 could induce significant reduction of HSV-1 viral load and titer in our *in vitro* proof-of-concept experiments, it is of utmost importance to verify that these potent cargos did not create undesired gene editing outcomes. Such off-target DNA cleavage could potentially give rise to chromosomal rearrangements and other deleterious effects that could lead to genomic instability.[24–26] To assess the specificity of ICP0g2 and ICP27g1, we performed GUIDE-seq,[27] a cell-based homology independent method to nominate potential genome-wide off-target sites, in our HSV-1 reporter cell line transfected with plasmids expressing SaCas9 with either ICP0g2 or ICP27g1. This tag-based method relies on non-homologous DNA end joining (NHEJ)-mediated integration of exogenously supplied blunt, double-stranded oligodeoxynucleotides (dsODNs) of defined sequence into double-stranded breaks within the cellular genome. GUIDE-seq analysis identified few nominated off-target sites for both ICP0g2 and ICP27g1 as determined by Unique Molecular Identifier (UMI) read count (Figures 2A and 2B; Tables 3, S1, and S2). Importantly, no sites with $\leq$3 total mismatches plus bulges were identified for either gRNAs (Table 3). Additionally, the total UMI read count at the ICP27g1 on-target site was >20,000 (Figure 2B; Table S2). However, at the ICP0g2 on-target site, the total read count was almost 70-fold lower (Figure 2A; Table S1), potentially due to the >85% GC-content in the surrounding region of this gRNA. The read count at the GUIDE-seq nominated sites was significantly lower than the read count at the on-target sites (Figures 2A and 2B). Together, the GUIDE-seq results suggested that the two SaCas9 gRNAs may pose minimal risk for off-target activity. However, further characterization of GUIDE-seq and *in silico* nominated off-target sites was necessary.

As a confirmation of the GUIDE-seq results, amplicon-seq was performed at a selection of GUIDE-seq ($\leq$5 total mismatches plus bulges) and *in silico* ($\leq$3 total mismatches plus bulges; Table 2) nominated off-target sites for ICP0g2 and ICP27g1 (Table S3). For ICP0g2, 15 out of 16 (93.75%) tested nominated off-target sites did not show significantly higher editing compared with the non-targeting control (Figure 2C). At one off-target site (OT1) of ICP0g2, which aligns to an intergenic region within chromosome 8, the editing was statistically significant, although the editing at this site was only 0.06%. For ICP27g1, 5 out of 6 (83.33%) tested nominated off-target sites did not show significantly higher editing compared with the non-targeting control (Figure 2D). At OT1 of ICP27g1, which primarily aligns to the intron of *ZNF331* within chromosome 19, the editing was 0.54% and statistically significant compared with the non-targeting control.

Figure 1. Different combinations of gRNAs targeting *ICP0* and *ICP27* reduce HSV-1 viral load and titer in Vero cells

(A) Effects of transient plasmid delivery of CRISPR-SaCas9 payload on HSV-1 viral load, which was measured by ddPCR of viral DNA probing for *UL28* and normalized to the *telomerase reverse transcriptase* (*TERT*) gene DNA sequence. (B) Effects of transient plasmid delivery of CRISPR-SaCas9 payload on HSV-1 viral titer, which was measured by plaque assay using supernatants from the same samples as in (A). In (A) and (B), four biological replicates were normalized to their respective internal controls and then plotted. (C) Schematic illustration of the SaCas9-g2g1 expression construct cloned in an AAV plasmid. (D) Effects of AAV2 transduction of CRISPR-SaCas9 payload on HSV-1 viral load. The MOIs of AAV2 vectors are 2E+4, 1E+5, and 5E+5 vg/cell. (E) Effects of AAV2 transduction of CRISPR-SaCas9 payload on HSV-1 viral titer. In (D) and (E), two biological replicates were normalized to their respective internal controls and then plotted. Results are presented as mean + SEM. Statistical significance was determined by two-tailed Student's t test: $^{**}p < 0.01$; $^{***}p < 0.001$; $^{****}p < 0.0001$. Note some data points are zero and are not shown on the plots with logarithmic scale.

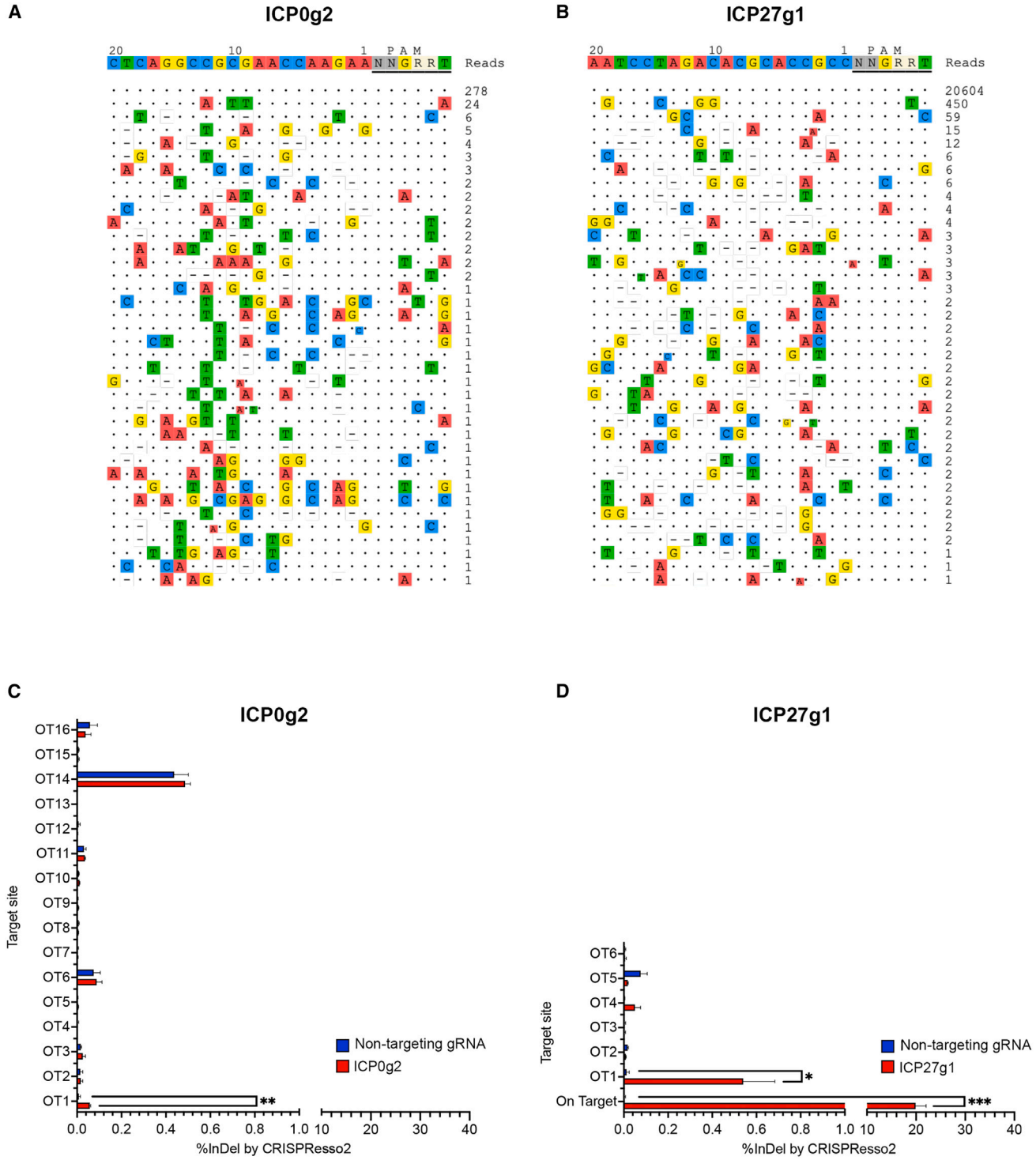

Figure 2. Off-target analysis of ICP0g2 and ICP27g1

(A) GUIDE-seq analysis of ICP0g2. (B) GUIDE-seq analysis of ICP27g1. In (A) and (B), sequences shown are the top 38 recovered sites based on UMI count. Underline indicates the PAM of the SaCas9 nuclease. Dots indicate matches with the cognate spacer sequence. Colored letters indicate mismatches with the cognate spacer sequence. Dashes indicate truncated sequences compared with the cognate spacer sequence. Small font letters indicate the inserted nucleotides compared with the cognate spacer sequence. (C) Quantification of editing activity by SaCas9 programmed with ICP0g2 at the top 16 GUIDE-seq and *in silico* nominated off-target sites in the

(legend continued on next page)

It is critical to note that these experiments were performed in HEK293FT transformed cells, which is not a clinically relevant cell type. Therefore, further characterization in primary cells and more therapeutically relevant model systems will be needed to confirm such off-target editing. Due to the observed *in vitro* efficacy and minimal off-target activity, these results prompted us to proceed with the *in vivo* proof-of-concept experiments.

Rabbit as a model for HSV-1 infection and reactivation

Since HSV-1 can be efficiently targeted with CRISPR-Cas9 in cells, we reasoned that targeting the HSV-1 viral genome *in vivo* could render the virus unstable, resulting in elimination of the latent viral reservoir in the TG. To test this hypothesis, we adapted our experiments to the rabbit keratitis model because HSV-1 infection in rabbit is more prototypical of human disease than that of other animal models.[28] Furthermore, the large size of the rabbit eyes makes virus inoculation and corneal examination simpler compared with mouse eyes, and it provides an abundant tear film for viral shedding analysis.

New Zealand White (NZW) rabbits were infected with HSV-1 strain 17Syn+ virus at 1.5E+5 pfu/eye through corneal scarification (Figure S3A). In this model, primary infection resolves within the first 2 to 3 weeks. At 4 weeks post-infection, latency has been established within the TG and no infectious virus can be detected in the ocular swabs.[28] To reactivate the virus from latency, a stress stimulus was applied in which each rabbit's eye received transcorneal iontophoresis of epinephrine (TCIE), a procedure in which a small electric current drives the uptake of epinephrine into the eye, for 3 consecutive days.[28,29] Plaque assay was used to measure virus reactivation by determining the presence or absence of infectious virus in the daily ocular swabs from each eye. As expected, we observed no infectious virus from ocular swabs of the non-TCIE-treated control group (Figure S3B). In contrast, we observed infectious virus from ocular swabs of all (12 of 12) TCIE-treated eyes. Two to six viral positive ocular swabs were observed from each reactivated eye (Table S4; Figure S3B). This finding confirmed that the rabbit keratitis model is an appropriate tool for modeling human HSV-1 infection and viral reactivation.

CRISPR-Cas9 gene editing reduced HSV-1 shedding in rabbits when delivered by corneal scarification

To assess the efficacy of our CRISPR-Cas9 gene editing strategy *in vivo*, we employed AAV vectors to deliver our payload to the latent rabbit keratitis model. First, we evaluated the ability of two neurotropic AAV serotypes, AAV8-Y733F and AAV9, to deliver SaCas9-g2g1 to the latent rabbit keratitis model via a corneal scarification route of administration (Figure 3A).[29,30] At 4 weeks post HSV-1 infection, AAV vectors were administered at a dose of 1E+11 vg/eye. After an additional 4 weeks, HSV-1 reactivation was induced by TCIE for 3 consecutive days. Viral shedding frequency was analyzed by the presence of infectious virus in the daily ocular swabs measured by plaque assay.

HSV-1 shedding frequency was presented as the percentage of swabs per eye that tested positive for the infectious virus (Figure 3B). Compared with the corresponding control groups, the rabbit eyes treated with the AAV8-Y733F or AAV9 vector expressing SaCas9-g2g1 experienced an ∼70% and ∼56% reduction in viral shedding, respectively (Figure 3B). More specifically, all rabbit eyes administered with the control vectors, AAV8-Y733F-EGFP or AAV9-SaCas9 scrambled, exhibited viral shedding (Table S5). In contrast, four out of eight eyes (50%) treated with AAV8-Y733F-SaCas9-g2g1, and 11 out of 18 eyes (61%) treated with AAV9-SaCas9-g2g1 showed no viral shedding, suggesting that CRISPR-Cas9 treatment suppressed virus reactivation. However, when we investigated AAV load in some of the rabbits' TG (Figures S4A and S4B) and cornea (Figures S4C and S4D), we detected few copies of AAV vector genomes (<0.1 copy/cell), suggesting that corneal scarification may not be an optimal route of administration for the delivery of our AAV9-CRISPR-Cas9 therapeutic payload to the TG. Therefore, additional routes of administration may need to be evaluated to improve the *in vivo* delivery efficacy in the rabbit keratitis model.

Intravenous administration of AIO AAV9-SaCas9-g2g1 vector eliminated HSV-1 viral shedding and reduced HSV-1 viral load in the TG of the latent rabbit keratitis model

To improve delivery of our therapeutic payload, we explored the use of i.v. administration and evaluated the efficacy of CRISPR-Cas9 in targeting the latent HSV-1 reservoir in the TG. We proceeded forward with AAV9 due to its wide use for systemic delivery and its high tropism for targeting the brain.[30,31] The AAV9 vector carrying SaCas9-g2g1 was administered to the rabbit keratitis model at an AAV dose of 6E+12 vg/kg (low dose) or 3E+13 vg/kg (high dose), through ear vein injection. After TCIE-induced viral reactivation, we first evaluated the viral shedding frequency in the rabbits' eyes. We observed that all eyes in the control groups (buffer and scrambled) exhibited HSV-1 shedding in the collected ocular tear swabs, except for one eye (Table S6). Remarkably, we observed that no eyes in the AAV9-SaCas9-g2g1 low-dose-treated group and only one eye in the high-dose treatment group exhibited viral shedding in the collected ocular tear swabs (Figure 4A; Table S6).

We next assessed if the absence of viral shedding in the treated groups correlated with a reduction in the HSV-1 viral load in the TG where the virus establishes lifelong latency. One random tissue sample from each group was removed from this analysis and kept for further characterization (data not shown), and the rest of the tissues were used for DNA and RNA extractions. We first analyzed HSV-1 DNA from the TG using two primer/probe sets targeting the *LAT* and *UL28* regions. We observed a 50% reduction in HSV-1 viral load relative to the

HEK293FT reporter cells. (D) Quantification of editing activity by SaCas9 programmed with ICP27g1 at the on-target site and top 6 GUIDE-seq and *in silico* nominated off-target sites in the HEK293FT reporter cells. Results were obtained from three independent experiments and presented as mean + SEM. Statistical significance is determined by two-tailed Student's t test: $^{*}p < 0.05$; $^{**}p < 0.01$; $^{***}p < 0.001$.

Table 3. Number of GUIDE-seq nominated off-target sites in the HEK293FT reporter cell line

Number of mismatches and bulges	1	2	3	4	5	6	Total
ICP0g2	0	0	0	1	6	31	**39**
ICP27g1	0	0	0	1	12	123	**137**

controls in both AAV9-SaCas9-g2g1-treated groups (Figures 4B and S5). Additionally, amplicon-seq analysis at the ICP27g1 target site showed mean InDel percentages of 0.78% and 1.65% in the low- and high-dose groups, respectively (Figure S6). During HSV-1 latent infection, *LAT* is the only highly expressed HSV-1 viral gene product.[32] Therefore, it is plausible that the reduction in HSV-1 viral DNA in the TG will lead to reduced *LAT* RNA. To test this hypothesis, we quantified the level of *LAT* RNA in the rabbit TG by reverse transcription digital PCR (RT-dPCR) analysis. Compared with the controls, the *LAT* RNA was reduced by 80% and 60% in the low-dose and high-dose treatment groups, respectively (Figure 4C).

Compared with corneal scarification, *in vivo* efficacy of AAV9-SaCas9-g2g1 was improved when delivered by i.v. administration, a finding we attributed to the efficient delivery of SaCas9 and gRNAs to the HSV-1 reservoirs. Therefore, we evaluated AAV load in the TG and cornea of the rabbits that were treated with AAV9-SaCas9-g2g1 delivered by i.v. administration. The AAV vector genome copies were quantified by dPCR. In the TG, rabbits that received a low dose of AAV9 vector had approximately one AAV copy per cell, while rabbits that received a high dose had approximately 10 AAV copies per cell (Figures S7A and S7B). In the cornea, rabbits that received a low dose had approximately 0.5 AAV copy per cell, while rabbits that received a high dose had about one AAV copy per cell (Figures S7C and S7D).

Finally, we evaluated expression of SaCas9 mRNA and gRNAs in the TG by RT-dPCR. The expression of all three RNAs was comparable between AAV low- and high-dose treatment groups, and there was a positive correlation in the expression of the SaCas9 mRNA and gRNAs (Figure S8). Importantly, we found that the TG corresponding to the singular eye that exhibited viral shedding in the high-dose treatment group (Figure 4A, Rabbit-9 OS, square cyan) had no detectable expression of SaCas9 mRNA or gRNAs. This finding was an anomaly. However, the volume for delivery of vector in the high-dose AAV group required multiple injections into both of the rabbit ear veins. Therefore, this finding could be a result of technical challenges in delivering large volumes into a single animal.

These results demonstrated that delivery of CRISPR-Cas9 by AAV9 vector using i.v. administration is effective in reaching the cornea, where the virus actively replicates, and the sensory neurons in the TG, where the virus establishes lifelong latency. Additionally, i.v. administration of 6E+12 vg/kg AAV9-SaCas9-g2g1 was effective in inhibiting HSV-1 shedding in the eyes and reducing the viral load in the TG of the latent rabbit keratitis model. Last, a single AAV copy per cell in the TG may be sufficient to completely abolish viral shedding and reduce viral load in the HSV-1 latent reservoir.

DISCUSSION

HSV-1 keratitis, a leading cause of infectious blindness worldwide, is caused by recurrent infections of the cornea by HSV-1. Currently, there is no approved cure or therapeutic vaccine for HSV-1 keratitis. Existing treatments with nucleoside analogs are primarily palliative. The rise of drug-resistant HSV-1 virus strains warrants significant attention from the research field. Several prophylactic and therapeutic vaccine candidates are currently under development.[33] Although a vaccine may reduce the frequency of viral reactivation and lesion outbreaks, it may not eliminate the latent HSV-1 virus.

Recent studies have shown that genome editing technologies, including CRISPR-Cas9 and meganuclease, can effectively inhibit viral replication and may potentially eradicate latent HSV-1 reservoirs. However, the gene therapies outlined in those studies may not be the most ideal therapeutic payload. First, recent studies have demonstrated robust and efficacious reduction of both genital and orofacial HSV-1 infection by AAV delivery of dual meganucleases.[11,12] Although they are compact and active, meganucleases can be complicated to engineer and may require extensive effort to improve potency and specificity. CRISPR-Cas9 systems have transformed the genome editing field by removing the need for extensive engineering to customize targeted DNA-binding proteins. Second, two independent groups have used lentiviral vectors to deliver CRISPR-Cas9 into the HSV keratitis mouse models.[13,34] Recently, one such study has been further carried out in a human clinical trial.[14] However, lentiviral vectors can present major safety risks due to insertional mutagenesis and large-scale lentiviral vector manufacturability remains unclear. Therefore, a scalable, effective, and safe treatment for HSV-1 keratitis that can prevent HSV-1 reactivation from latency is needed.

In this study, we applied CRISPR-SaCas9 to target and disrupt *ICP0* and *ICP27*, two critical genes in the HSV-1 genome, proposing a potential curative therapeutic approach for HSV-1 keratitis. In our *in vitro* experiments, we demonstrated that our therapeutic approach can successfully inhibit viral infection in cell culture. Transient expression of SaCas9 and the paired gRNAs, delivered via plasmids, in Vero cells resulted in a significant reduction in HSV-1 viral load and titer. Furthermore, transduction with AIO AAV2 vector nearly abolished the virus *in vitro*. In our *in vivo* experiments, we demonstrated that the delivery of SaCas9-g2g1 with AAV9 vector via i.v. administration led to a reduction of 50% in HSV-1 viral DNA and a reduction of 60%–80% in *LAT* RNA in the TG of treated rabbits. These reductions resulted in complete elimination of viral shedding

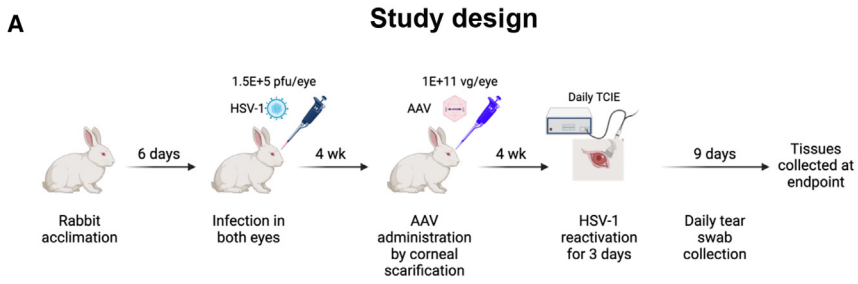

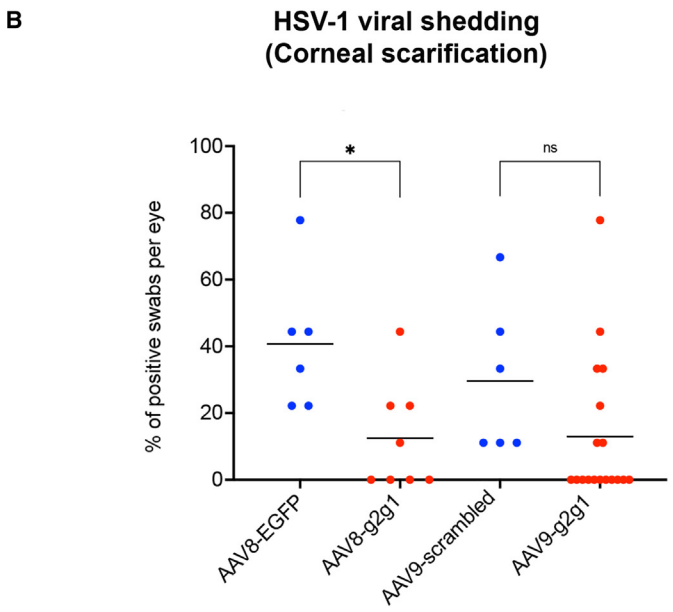

Figure 3. AAV-SaCas9-g2g1 vectors delivered by corneal scarification reduce viral shedding in the latent rabbit keratitis model

(A) Schematic representation of experimental design and timeline of ocular infection with HSV-1 and treatment with AAV-SaCas9-g2g1 vectors delivered by corneal scarification. (B) HSV-1 virus shedding frequency in tear swabs presented as the percentage of infectious viral positive swabs per eye. Results are presented as individual points with mean. Statistical significance is determined by two-tailed Student's t test: $^{*}p < 0.05$.

from rabbits' tears, except in one eye, which showed no expression of SaCas9 mRNA and the guide RNAs in the corresponding TG. This would fully eliminate the risk of viral transmission, since the transmission and spread of the virus from infected individuals to healthy subjects is one of the big concerns of the disease.[35]

AAV load analysis (measured by dPCR) revealed that rabbits that received a low dose of the AAV9 vector had approximately one AAV copy per cell in the TG. This level of the AAV9-SaCas9-g2g1 vector resulted in a 50% reduction in HSV-1 DNA, an 80% reduction in *LAT* RNA, and complete elimination of viral shedding in the eyes. Previous studies have shown that HSV-1 establishes latency in neurons,[36,37] which make up about 10% of the cell population in the TG.[38,39] The remaining 90% predominantly consists of glial cells, such as satellite glial cells and Schwann cells. AAV9 is relatively effective at transducing peripheral neurons, but it has limited efficiency for glial cells in the peripheral nervous system.[40] In addition to this, other labs, including the Neumann and Bloom labs have shown using indirect immunofluorescence that AAV vectors co-localize with HSV-1 in the neuron.[29,41,42] Given this information, our findings suggest that the low dose of the AAV9 vector could potentially lead to delivery of more than one AAV copy per TG neuron. Additionally, the high dose of the AAV9 vector resulted in approximately 10 AAV copies per cell. However, the higher AAV load in the TG did not result in a greater reduction in HSV-1 DNA and *LAT* RNA in the TG, or viral shedding in the eyes. It is likely that the low dose of the AAV9 vector (6E+12 vg/kg) is sufficient to reach saturating expression of CRISPR-Cas9 payload in HSV-1-infected TG neurons, and increasing the dose of the AAV9 vector would not lead to higher activity. Within the HSV-1-infected and AAV9-transduced TG neurons, only a few copies of the AAV9 vector might be required to inactivate the latent HSV-1 DNA. Additionally, we observed a higher reduction in *LAT* RNA than in HSV-1 DNA, which suggests that the remaining HSV-1 DNA in the TG may have undergone repair and possesses gene editing outcomes (InDel or excision) that hinder the ability to transcribe *LAT* RNA and/or reactivate the virus. Preliminary analysis of the HSV-1 DNA in the TG showed mean InDel percentages of approximately 1% at the ICP27g1 target site. Furthermore, ICP0g2 amplicon proved to be challenging to amplify and sequence due to the high GC-content surrounding the target site (>85%). It is important to note that InDel analysis was performed on tissues at 40 days post AAV9 administration and 12 days post TCIE treatment. Because the HSV-1 DNA in the TG is present as a nonreplicating circular episomal form,[43] it is possible that at this late time point, the majority of the DNA that received two or three double-stranded breaks induced by CRISPR-Cas9 was not repaired properly or recircularized, and was therefore degraded and not present for our InDel analysis. The HSV-1 DNA analyzed by amplicon-seq at the endpoint was likely either unedited DNA or DNA that was repaired by the cellular machinery. Analyzing at an earlier time point might reveal higher InDel rates. Future work will focus on better understanding the percentage of HSV-1 infected TG neurons that are transduced by AAV9 vectors

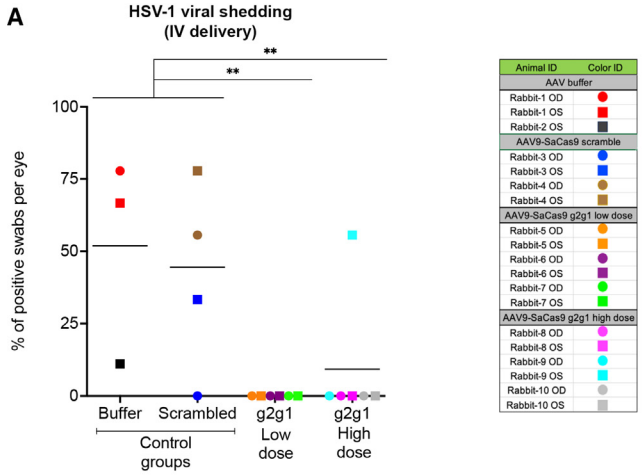

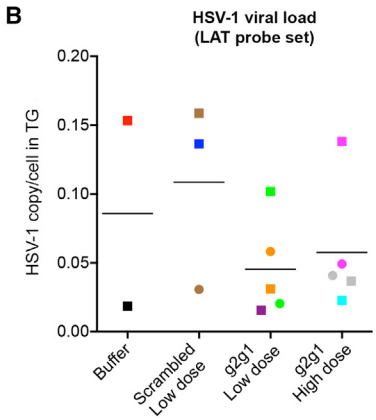

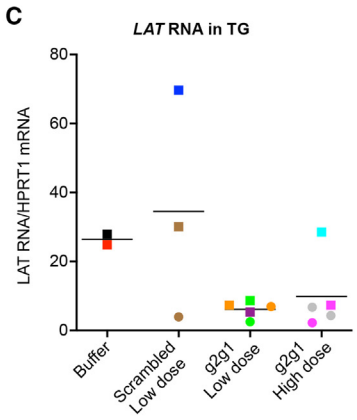

Figure 4. AAV-SaCas9-g2g1 vector delivered by i.v. administration eliminates viral shedding and reduces viral load in the latent rabbit keratitis model

(A) HSV-1 virus shedding frequency in tear swabs presented as the percentage of infectious viral positive swabs per eye. The eye IDs are shown in the table on the right. Circles: right eyes (OD), squares: left eyes (OS). The two eyes from the same rabbit are represented with the same color. The right eye of Rabbit-2 from the buffer group did not receive TCIE due to cornea opacity, and the shedding data were not included for this eye. Results are presented as individual points with mean. Statistical significance is determined by two-tailed Student's t test: $^{**}p < 0.01$. (B) HSV-1 viral load in the rabbit TG as measured by dPCR of viral DNA probing for the HSV-1 *LAT* sequence and normalized to the rabbit *TERT* DNA. (C) The level of *LAT* RNA in the rabbit TG as measured by RT-dPCR. The level of *LAT* RNA was normalized to the level of rabbit *HPRT1* mRNA.

in the latent rabbit keratitis model, the influence of different CRISPR-Cas9 editing events in the TG neurons, and the viral load reduction threshold needed for a "functional cure."

AAV vectors have shown promise in gene therapy, and numerous preclinical and clinical studies have demonstrated their good safety profile particularly in comparison with other gene therapy vectors.[44] However, at high doses, AAV vectors can induce serious adverse events, such as thrombotic microangiopathy and hepatotoxicity.[45–47] Moreover, AAV toxicity can cause neuronal injury in both animal models and humans.[45,48–50] Fortunately, one encouraging finding in our study is the high effectiveness of our AAV9-SaCas9-g2g1 vector with the low dose (6E+12 vg/kg) in inhibiting HSV-1 shedding in rabbits. This dose is more than 16 times lower than the 1E+14 vg/kg dose used in several ongoing AAV gene therapy trials, suggesting a safe and potentially cost-effective therapy for the patients. It has also been reported that AAV vectors can integrate into the CRISPR-Cas9-induced DNA breaks, raising significant safety concerns.[51] However, the HSV genome does not integrate into the host genome but persists as a circular episomal form during latency. It is unknown if the AAV vector will be integrated into the HSV-1 DNA-induced breaks. In theory, AAV integration into the HSV genome will not pose significant safety risks. However, more in-depth analysis is warranted to ensure the safety of our delivery modality.

While our therapeutic approach shows promise, there is room for improvement. For example, in our study, we only evaluated AAV delivery via two administration routes, corneal scarification and i.v. administration. Future studies may explore alternative or combined routes for safer and more efficient delivery of the therapeutic payload. Moreover, while AAV vectors are widely used in gene therapy, emerging research into non-viral delivery methods shows great potential in terms of safety and efficacy. However, much remains unknown about targeting non-viral vectors to the peripheral nervous system (PNS). Last, we observed editing at a single nominated off-target site for each gRNA (OT1 of ICP0g2 – 0.06%; OT1 of IC27g1 – 0.54%). OT1 of ICP0g2 aligns to an intergenic region within chromosome 8. OT1 of ICP27g1 primarily aligns to the intron of multiple transcript variants of *ZNF331*. However, it does map to the first exon in one transcript variant. *ZNF331* encodes for a transcriptional repressor that is frequently methylated in human esophageal, gastric, and colorectal cancer.[52–54] While such activity may warrant some concern, it is critical to note that these off-target assessment activities were performed in a transformed mammalian cell line. Additional characterization in therapeutically relevant primary cells is critical to ascertain the genotoxic potential of SaCas9-g2g1. Furthermore, we can apply methods to improve our specificity of our therapeutic payload, including gRNA modification or use of high-fidelity SaCas9 variants.[55–57] Additionally, identifying more specific and potent guide RNAs for SaCas9 or other Cas endonucleases will enhance the safety of CRISPR-Cas gene editing therapy. Nonetheless, we believe that our CRISPR-Cas9 gene editing approach

has the potential to be a curative therapeutic application for HSV-1 keratitis.

In conclusion, we present a proof-of-principle study for a CRISPR-Cas9-based therapy with potential to eradicate latent HSV-1 infections in HSV-1 keratitis. Our CRISPR-Cas9 gene editing approach may be applicable to the treatment of other HSV-1 related diseases, such as herpes labialis, herpes simplex encephalitis, and genital herpes. Additionally, identifying robust and safe gRNAs that are conserved in both HSV-1 and HSV-2, will enable the use of a single gene therapy product for all herpes diseases. This "one drug fits all" strategy would significantly reduce the development cost for various herpes diseases.

MATERIALS AND METHODS

HSV-1 genome library construction and consensus sequence generation

An internal HSV-1 genome library was created with the HSV-1 genome sequences. Strain information and coding sequence (CDS) fasta sequences for the HSV-1 were downloaded from the ViPR database (https://www.bv-brc.org/view/Virus/10239; Version Feb 2022; 46,027 strains and 62,554 GenBank IDs). The GenBank IDs and CDS fasta sequences were filtered using the 9,409 GenBank IDs obtained from the NCBI Nucleotide database using the keyword "human alphaherpesvirus 1."

To identify the CDS sequences for the *ICP0* and *ICP27* genes in different HSV-1 strains, the HSV-1 strains and GenBank IDs containing "ICP0$|ICP0.|RL2$|RL2." and "ICP27$|ICP27.|UL54$|UL54." were identified from the HSV-1 genome library and labeled as *ICP0* and *ICP27*, respectively. The percentage of guide conservation was calculated by dividing the strain counts for each guide RNA by the total strain counts of the *ICP0* or *ICP27* in the database.

To build the *ICP0* and *ICP27* consensus sequences, all CDS fasta sequences for *ICP0* and *ICP27* genes were fetched, and a multiple sequence alignment (MSA) was built separately for *ICP0* and *ICP27* using the Clustal Omega alignment (ClustalOmegaCommandLine package of BioPython). A consensus sequence was built based on the MSA using the AlignIO package of BioPython. The threshold parameter was set to 0.5, which determines the base to be added per position of the consensus sequence. If the percentage of the most common base was greater than 50%, then that base was added, otherwise an ambiguous character (N) was added. A position-specific scoring matrix (PSSM) was generated and the consensus bases that were observed in at least 25% of CDS sequences were selected to form the final consensus sequences.

In silico off-target analysis

In silico off-target analysis of the selected SaCas9 gRNA sequences was obtained using an in-house-developed Nextflow pipeline. Briefly, we utilized BWA aln tool to select for genomic sites in the hg38 genome with homology to the guide sequence, CasOFFinder tool[23] to obtain all possible guide/target sequence alignments at the selected sites, and a downstream post-processing step to select for sites with up to

(1) 1 mismatch + 1 bulge in guide sequence.
(2) 2 mismatches + 1 bulge in guide sequence.
(3) 3 mismatches + 1 bulge in guide sequence.
(4) 4 mismatches + 0 bulge in guide sequence.
(5) 5 mismatches + 0 bulge in guide sequence.

CasOFFinder run was done using the "NNGRRN" PAM sequence and allowing for up to five mismatches and one bulge. The identified sites were clustered by assigning a cluster ID based on PAM position if the identified genomic coordinates of the *in silico* site PAM start positions are within 5 bp distance. Clustered sites were deduplicated based on the cluster ID by selecting the lowest total mismatch/bulge in guide sequence, lowest bulge in guide sequence, and lowest mismatch in guide sequence.

Design of HSV-1 reporter construct and generation of HSV-1 HEK293FT stable reporter cell line

The HSV-1 reporter construct consists of two cassettes flanked by two AAVS1 CRISPR target sites (Figure S2B). The first cassette is used to screen for the construct integration and includes a PGK promoter driven EGFP, followed by a P2A self-cleaving peptide, a puromycin-resistant gene, and human growth hormone (hGH) polyA signal. The second cassette contains the HSV-1 consensus sequences for *ICP27* and *ICP0* flanking a minCMV-mTagBFP2-PEST-BGH pA cassette. This construct was synthesized at GenScript. To generate the HSV-1 knockin reporter cells, 0.5 μg of the construct and 20 pmol of RNP complex of SpCas9 and AAVS1 gRNA (Synthego) were nucleofected into 2.5E+5 HEK293FT cells (Thermo Fisher Scientific). Nucleofection was performed using 4D-Nucleofector System (Lonza), SF Cell Line Kit S, and the CM-130 program following the manufacturer's protocol. Four days after nucleofection, the media was removed, and fresh media containing 0.5 μg/mL of puromycin dihydrochloride (Thermo Fisher Scientific) was added to the cells. Ten days post-selection, cells were collected, and single-cell clones were established by serial dilution in 96-well plates. A single-cell clone containing over 95% EGFP-positive cells was selected for further expansion and used in the current study.

Plasmid transfection in HSV-1 HEK293FT reporter cells

HSV-1 HEK293FT reporter cells were seeded in 24-well plates (Thermo Fisher Scientific) and cultured in Dulbecco's modified Eagle's media (DMEM; Thermo Fisher Scientific) supplemented with 10% fetal bovine serum (FBS; Thermo Fisher Scientific) for 24 h in a 37°C incubator with 5% CO_2. At approximately 70% confluency, the cells were transfected with 500 ng of plasmid DNA and Lipofectamine 3000 (Thermo Fisher Scientific) following the manufacturer's directions. The cells were collected 72 h post transfection for DNA analysis.

Analysis of the gRNA pairs-induced excision in the reporter cell line

Genomic DNA was extracted from HSV-1 HEK293FT reporter cells transfected for 72 h with the six gRNA pairs targeting *ICP0* and *ICP27* genes. A total of 50 ng of genomic DNA was used for PCR amplification with high-fidelity Primestar GXL-DNA polymerase (Takara Bio)

and the HSV-1 Excision Forward and HSV-1 Excision Reverse primers listed in Table S7, which anneal in regions that encompass all target sites in *ICP0* and *ICP27*. Ten microliters of the PCR products were used for agarose gel electrophoresis and the excision bands were determined based on their predicted sizes.

Plasmid transfection in Vero cells

Vero cells (ATCC, CCL-81) were seeded in six-well plates (Thermo Fisher Scientific) and cultured in DMEM supplemented with 10% FBS for 24 h in a 37°C incubator with 5% CO_2. At approximately 70% confluency, the cells were transfected with 2 μg of plasmid DNA and Lipofectamine 3000 (Thermo Fisher Scientific) following the manufacturer's directions.

HSV-1 infection in Vero cells

Vero cells were infected 48 h post plasmid transfection with HSV-1 17Syn+ virus resuspended in Opti-MEM media (Theromo Fisher Scientific) for 3 h at an MOI of 5E−4 pfu per cell. HSV-1-containing Opti-MEM media was then removed, the cells were washed with phosphate-buffered saline (PBS) and cultured in fresh 500 μL of DMEM supplemented with 10% FBS media for 48 h. Supernatants were used for plaque assay analysis, and cells were collected for DNA analysis.

Design of scrambled gRNA controls

The scrambled gRNAs controls (ICP0g2-scrambled, ACAUCAA GCGCCGAGCGAAC; ICP27g1-scrambled, GCCAGCGCAACA CACAUCUC) were designed by shuffling the spacer sequences of ICP0g2 and ICP27g1. Our internal CasOFFinder tool was used to confirm that there were no genomic targets with two mismatches and one bulge or with three mismatches without bulge in the human genome, African green monkey genome (for Vero cells), or rabbit genome.

Production of AAV vectors

The AIO AAV2-SaCas9-g2g1 and scrambled vectors were prepared at PackGene Biotech. The AAV8-Y733F-EGFP and AAV8-Y733F-SaCas9-g2g1 vectors were prepared at the University of Florida Ocular Gene Therapy Core. The AAV9-SaCas9-g2g1 and scrambled vectors were prepared at the University of North Carolina Vector Core. All these AAV vectors were produced using triple plasmid transfection in adherent HEK293 cells. Subsequently, the AAV vectors were purified using iodixanol density gradient centrifugation and formulated in PBS containing 0.001% pluronic F-68. The titers of the vectors were determined using QIAcuity digital PCR (Qiagen) with two primer/probe sets targeting the CMV promoter and the SV40 polyA sequences. The primer and probe sequences are listed in Table S7. The average titer was used in the experiments.

Transduction of Vero cells with AAV2-SaCas9 vectors and HSV-1 infection

Vero cells were seeded in 12-well plates and cultured in DMEM supplemented with 10% FBS for 24 h. At approximately 70% confluency, the cells were transduced with AAV2-SaCas9-g2g1 or scrambled vector at different MOIs. After 48 h, the cells were infected with HSV-1 strain 17Syn+ virus for 3 h at an MOI of 5E−4 pfu per cell. The virus-containing media was then removed and replaced with fresh culture media. Forty-eight hours later, the cells were collected for DNA analysis, and the supernatants were used for plaque assay analysis.

ddPCR analysis

Genomic DNA was isolated from Vero cells using the NucleoSpin Tissue, Mini kit for DNA from cells and tissue (MACHEREY-NAGEL) following the provided instructions. ddPCR was performed using the 2X ddPCR Supermix for Probes (No dUTP) in the QX200 Droplet Digital PCR system (Bio-Rad Laboratories; data in Figure 1). A total of 500 pg of genomic DNA was used as a template with the following thermal cycling conditions: 95°C for 10 min, followed by 40 cycles of 94°C for 30 s and 60°C for 1 min, and final incubation at 98°C for 10 min. Data acquisition and analysis were conducted using the QX200 droplet reader and QuantaSoft software provided with the instrument. The number of HSV-1 copies in the Vero cells was quantified using a primer/probe set targeting the HSV-1 *UL28* gene,[58] which is approximately 49 kb and 68 kb away from each copy of the duplicated ICP0g2 target sites, and approximately 61 kb away from the ICP27g1 target site. The HSV-1 copy numbers were normalized to the copy number of the endogenous *TERT* gene DNA sequence to calculate the HSV-1 copy numbers per cell.

Plaque assay for the Vero cell supernatants

The infectious titers of HSV-1 were determined using plaque assay. Vero cells were grown in a 24-well plate until they reached 100% confluence. The cells were then treated with HSV-1 virus-containing supernatants at different dilutions. After a 3-h incubation with the virus, the viral inoculum was removed, and the cells were overlaid with 500 μL of a 0.4% methyl cellulose (MilliporeSigma) in complete culture medium to allow only cell-to-cell spread of the virus. Two days after HSV-1 infection, the Vero cells were fixed with 5% Trichloroacetic acid (TCA; MilliporeSigma) for 10 min at room temperature. The cells were then stained with 0.05% crystal violet in a mixture of 25% methanol and 75% water for 15 min at room temperature. The staining was washed off with running water, and the 24-well plate was left to dry overnight at room temperature. The plaques in each well were counted individually. The dilutions that resulted in fewer than 100 plaques per well were used to determine the infectious titers.

GUIDE-seq analysis

We performed GUIDE-seq experiment with some modifications to the original protocol.[27] Briefly, in 24-well plates, HEK293FT reporter cells were transfected with 400 ng of Cas9 plasmids and 7.5 pmol of annealed GUIDE-seq oligonucleotide using Lipofectamine 3000 transfection reagent (Thermo Fisher Scientific) according to the manufacturer's protocol. Genomic DNA was extracted at 72 h after transfection. Library preparations were conducted according to protocols described previously,[27] and quantified by a 4150 TapeStation System (Agilent) and Qubit 4.0 (Thermo Fisher Scientific). Equal amounts were pooled and sequenced on Illumina MiSeq instrument using a MiSeq reagent kit v2 (300 cycles).

The raw sequencing data were analyzed using an in-house developed Nextflow bioinformatics pipeline, which is based on the GUIDE-seq analysis code[27] with some modifications.

The raw sequencing reads were demultiplexed using deML tool (https://github.com/grenaud/deML) by allowing up to two mismatches in the barcode sequences. After UMI tagging and consolidation of reads that share the same UMI, the paired end reads were aligned to the hg38 reference genome using the BWA-MEM algorithm with default parameters. During identification of dsODN integration sites, different from the published pipeline, dsODN primers were searched across the reads with up to two mismatches allowance. This approach allows identification of primer sequences, which have sequencing errors. Identified sites were realigned using Calitas tool, but using ±20 bp window at the identified dsODN integration genomic coordinate. Mosdepth tool was used to calculate base coverage at the identified sites and provided *in silico* off-target sites. Annotations, such as gene names, descriptions, phenotypes, TSG overlaps, and locations, were prepared for the identified sites. The results of identified sites, target annotations, Calitas alignments, and read QC and genome coverage were sent to AWS S3 bucket locations. An AWS Athena database and corresponding tables were created for the output results. The downstream analysis was performed using Tableau software by connecting to the AWS Athena database.

Targeted amplicon deep sequencing and data analysis

Regions flanking each target site were PCR-amplified using Q5 High-Fidelity 2x Master Mix (New England Biolabs) for 30 cycles. For barcoding PCR, 0.5 μL of each reaction was amplified for 10 cycles with barcoded primers to reconstitute the TruSeq adaptors. Equal amounts of the barcoded PCR products were pooled and purified with 0.7× SPRIselect bead-based reagent (Beckman Coulter), washed twice with 80% ethanol, and eluted in 30 μL of 1× TE buffer. Sequencing of the pooled amplicons was performed using MiSeq reagent kit v2 (500 cycles; Illumina) following the manufacturer's protocol.

MiSeq data analysis for indel frequencies at the on-target and off-target sites was performed using the CRISPResso2 software (*CRISPResso –fastq_r1 –fastq_r2 –amplicon_seq –guide_seq –ignore_substitutions –plot_window_size 20 –window_around_sgrna 5*.[59] "*–fastq_r1*" and "*–fastq_r2*" denote the r1 and r2 Fastq files that are output from the MiSeq machine. "*–amplicon_seq*" and "*–guide_seq*" are the input anticipated amplicon and guide RNA sequence. "*–cleavage_offset*" is the center of quantification window to use within respect to the 3′ end of the provided sgRNA sequence. "*–ignore_substitutions*" is used to ignore subtitutions around the cleavage positions as these may be caused by sequencing error. "*–plot_window_size*" defines the size of the window extending from the quantification window center to plot. "*–window_around_sgrna*" defines the size (in base pairs [bp]) of the quantification window extending from the position specified by the "–cleavage_offset" parameter in relation to the provided guide RNA sequence(s) (–guide_seq). Mutations within this number of bp from the quantification window center are used in classifying reads as modified or unmodified.

Latent rabbit keratitis model

Rabbit keratitis study was completed as previously described[42] with some modifications. New Zealand White (NZW) rabbits were anesthetized using intramuscular injections of ketamine (MilliporeSigma; 30 to 45 mg/kg) and xylazine (MilliporeSigma; 7.5 to 11.5 mg/kg). Rabbits were then infected with the HSV-1 strain 17Syn+ virus at a concentration of 1.5E+5 pfu/eye in a volume of 15 μL directly onto the cornea following light corneal scarification in a 2 × 2 crosshatch pattern. Rabbits were monitored daily for health and signs of blepharitis and conjunctivitis. Eyes were cleaned daily with saline solution. Slit lamp exams were performed every 2–3 days during this acute infection stage to assess ocular lesions. Rabbits that exhibited acute lesions with subsequent recovery were considered latently infected and used for further procedures. Four weeks later, 1E+11 vg of AAV vectors in 30 μL were administered by corneal scarification into each eye. For the i.v. administration, 6E+12 vg/kg or 3E+13 vg/kg of AAV was injected into one or both of the rabbit ear veins, depending on the dosing volume. Four weeks after AAV administration, HSV-1 reactivation was induced by TCIE for 3 consecutive days as described previously.[42] Swabbing was conducted daily from each eye, starting on the first day of TCIE and continuing for 12 days. The applicators containing the ocular swabs were placed in a tube containing 1 mL of sterile DMEM supplemented with 1% FBS and 1% antibiotic/antimycotics and stored at −80°C for a minimum of 48 h. Animals were humanely euthanized 9 days after the last TCIE, and tissues were collected and snap frozen for further analysis.

Protocols for the rabbit ocular infection experiments were approved by the University of Wisconsin-Madison Institutional Animal Care and Use Committee.

Plaque assay for ocular swab samples

Vero cells were seeded in a 24-well plate and incubated for 24 h until they reached approximately 90% confluence. The tubes containing the daily ocular swabs were thawed at 37°C. Next, the normal growth media was removed from the Vero cells, and the media from each ocular swab tube was transferred to individual wells. The plate was then incubated at 37°C with 5% CO_2 for 7 days. Finally, the individual wells were examined under a microscope to determine the presence or absence of plaques daily beginning at 24 h post-plating. In total, 12 consecutive days of ocular swab samples for each rabbit eye were analyzed. The samples from day 1, day 11, and day 12 were negative for all the rabbit eyes. These results were not included in the figures and tables.

Genomic DNA extraction from rabbit tissues

Rabbit tissues were mechanically homogenized in lysis buffer with the Bead Ruptor homogenizer (Omni International) as described by the manufacturer. The genomic DNA was extracted using Maxwell RSC Instrument with the tissue DNA kit following the manufacturer's protocol (Promega). In the corneal scarification study, genomic DNA extractions were performed on two right TGs in the control group, three right TGs in the AAV8-g2g1 group, and seven right TGs in

the AAV9-g2g1 group. In the i.v. delivery study, each TG was divided into halves, with each half used for either DNA or RNA extraction. Two TGs from the buffer group and three TGs from the scrambled group served as controls, while five TGs from both the g2g1 low-dose and high-dose groups were used for DNA and RNA analyses.

Total RNA extraction from rabbit tissues

Rabbit tissues were preserved in RNAlater after collection, and the tissues were homogenized with the Bead Ruptor homogenizer (Omni International). Total RNAs from tissue homogenates were extracted with RNeasy Plus kit following the manufacturer's protocol (Qiagen).

Reverse transcription

A total of 100 ng of total RNA from rabbit tissues was used for cDNA synthesis using SuperScript IV VILO Master Mix with ezDNase (Thermo Fisher Scientific) in a 20-μL reaction as described by the manufacturer. The cDNA was then diluted 10-fold or more, dependent on the target, for analysis with dPCR.

dPCR analysis

Analysis of DNA or cDNA from tissue samples was performed using the QIAcuity digital PCR system from Qiagen (data in Figures 4, S3–S5, and S7). DNA (between 4 and 40 ng) or diluted cDNA was used as a template for amplification using the following conditions: 95°C for 2 min, followed by 40 cycles of 95°C for 15 s and 60°C for 1 min. Data acquisition and analysis were conducted from the same instrument as described by the manufacturer (Qiagen). The primers and probes used for dPCR are listed in Table S7. The LAT primer/probe set targets a location about 2 kb upstream of the nearest copy of the duplicated ICP0g2 target sites and approximately 4.5 kb downstream of the ICP27g1 target site.

DATA AND CODE AVAILABILITY

The raw and analyzed datasets from this study are available upon reasonable request to the corresponding author.

SUPPLEMENTAL INFORMATION

Supplemental information can be found online at https://doi.org/10.1016/j.omtm.2024.101303.

ACKNOWLEDGMENTS

This work was mainly supported by funding from Excision BioTherapeutics, and in part by an unrestricted grant from Research to Prevent Blindness, Inc. to the University of Wisconsin-Madison Department of Ophthalmology and Visual Sciences to support institutional research facilities, and in part by the Core Grant for Vision Research from the NIH to the University of Wisconsin-Madison (P30 EY016665) (D.N.) to support institutional core facility services. M.S. was partially supported by funding from the NIH T32 training grant (2TL1TR002375-06). We express our gratitude to all members of Excision BioTherapeutics, especially Sivapalasingam S., Zhao H., Huo W., Arif A., Cradick T., Takeuchi R., and Slattery S., for their valuable discussions, advice, and insightful feedback.

AUTHOR CONTRIBUTIONS

Study design or conception: N.A., K.L., M.I., K.K., I.K.S., D.N., J.G., and G.-X.R. Performed experiments and/or data analysis: N.A., K.L., P.S., M.S., M.I., M.D., A.B., and G.-X.R. Methodology: N.A., K.L., P.S., M.S., M.I., M.D., A.B., I.K.S., D.N., J.G., and G.-X.R. Manuscript writing and preparation: N.A., K.L., M.I., and G.-X.R.

DECLARATION OF INTERESTS

N.A., K.L., M.I., J.G., and G.-X.R. are employees of Excision BioTherapeutics. K.K. is a co-founder, board member, scientific advisor, and holds equity in Excision BioTherapeutics. The authors have filed a patent application related to this work.

REFERENCES

1. James, C., Harfouche, M., Welton, N.J., Turner, K.M., Abu-Raddad, L.J., Gottlieb, S.L., and Looker, K.J. (2020). Herpes simplex virus: global infection prevalence and incidence estimates, 2016. Bull. World Health Organ. *98*, 315–329. https://doi.org/10.2471/BLT.19.237149.

2. Labib, B.A., and Chigbu, D.I. (2022). Clinical Management of Herpes Simplex Virus Keratitis. Diagnostics *12*, 2368. https://doi.org/10.3390/diagnostics12102368.

3. Bello-Morales, R., Andreu, S., and Lopez-Guerrero, J.A. (2020). The Role of Herpes Simplex Virus Type 1 Infection in Demyelination of the Central Nervous System. Int. J. Mol. Sci. *21*, 5026. https://doi.org/10.3390/ijms21145026.

4. Ahmad, B., and Patel, B.C. (2024). Herpes Simplex Keratitis (StatPearls).

5. Koganti, R., Yadavalli, T., and Shukla, D. (2019). Current and Emerging Therapies for Ocular Herpes Simplex Virus Type-1 Infections. Microorganisms *7*, 429. https://doi.org/10.3390/microorganisms7100429.

6. van Velzen, M., Ouwendijk, W.J.D., Selke, S., Pas, S.D., van Loenen, F.B., Osterhaus, A.D.M.E., Wald, A., and Verjans, G.M.G.M. (2013). Longitudinal study on oral shedding of herpes simplex virus 1 and varicella-zoster virus in individuals infected with HIV. J. Med. Virol. *85*, 1669–1677. https://doi.org/10.1002/jmv.23634.

7. Oseso, L., Magaret, A.S., Jerome, K.R., Fox, J., and Wald, A. (2016). Attitudes and Willingness to Assume Risk of Experimental Therapy to Eradicate Genital Herpes Simplex Virus Infection. Sex. Transm. Dis. *43*, 566–571. https://doi.org/10.1097/OLQ.0000000000000493.

8. Zhang, Y., and Li, M. (2021). Genome Editing Technologies as Cellular Defense Against Viral Pathogens. Front. Cell Dev. Biol. *9*, 716344. https://doi.org/10.3389/fcell.2021.716344.

9. Tripathi, S., Khatri, P., Fatima, Z., Pandey, R.P., and Hameed, S. (2022). A Landscape of CRISPR/Cas Technique for Emerging Viral Disease Diagnostics and Therapeutics: Progress and Prospects. Pathogens *12*, 56. https://doi.org/10.3390/pathogens12010056.

10. Roehm, P.C., Shekarabi, M., Wollebo, H.S., Bellizzi, A., He, L., Salkind, J., and Khalili, K. (2016). Inhibition of HSV-1 Replication by Gene Editing Strategy. Sci. Rep. *6*, 23146. https://doi.org/10.1038/srep23146.

11. Aubert, M., Strongin, D.E., Roychoudhury, P., Loprieno, M.A., Haick, A.K., Klouser, L.M., Stensland, L., Huang, M.L., Makhsous, N., Tait, A., et al. (2020). Gene editing and elimination of latent herpes simplex virus in vivo. Nat. Commun. *11*, 4148. https://doi.org/10.1038/s41467-020-17936-5.

12. Aubert, M., Haick, A.K., Strongin, D.E., Klouser, L.M., Loprieno, M.A., Stensland, L., Santo, T.K., Huang, M.L., Hyrien, O., Stone, D., and Jerome, K.R. (2022). AAV-delivered gene editing for latent genital or orofacial herpes simplex virus infection reduces ganglionic viral load and minimizes subsequent viral shedding in mice. Preprint at bioRxiv. https://doi.org/10.1101/2022.09.23.509057.

13. Yin, D., Ling, S., Wang, D., Dai, Y., Jiang, H., Zhou, X., Paludan, S.R., Hong, J., and Cai, Y. (2021). Targeting herpes simplex virus with CRISPR-Cas9 cures herpetic stromal keratitis in mice. Nat. Biotechnol. *39*, 567–577. https://doi.org/10.1038/s41587-020-00781-8.

14. Wei, A., Yin, D., Zhai, Z., Ling, S., Le, H., Tian, L., Xu, J., Paludan, S.R., Cai, Y., and Hong, J. (2023). In vivo CRISPR gene editing in patients with herpetic stromal keratitis. Mol. Ther. *31*, 3163–3175. https://doi.org/10.1016/j.ymthe.2023.08.021.

15. Wang, G., Zhao, N., Berkhout, B., and Das, A.T. (2016). CRISPR-Cas9 Can Inhibit HIV-1 Replication but NHEJ Repair Facilitates Virus Escape. Mol. Ther. *24*, 522–526. https://doi.org/10.1038/mt.2016.24.

16. Yoder, K.E., and Bundschuh, R. (2016). Host Double Strand Break Repair Generates HIV-1 Strains Resistant to CRISPR/Cas9. Sci. Rep. *6*, 29530. https://doi.org/10.1038/srep29530.

17. Liu, Y., Jeeninga, R.E., Klaver, B., Berkhout, B., and Das, A.T. (2021). Transient CRISPR-Cas Treatment Can Prevent Reactivation of HIV-1 Replication in a Latently Infected T-Cell Line. Viruses *13*, 2461. https://doi.org/10.3390/v13122461.

18. Wang, Z., Pan, Q., Gendron, P., Zhu, W., Guo, F., Cen, S., Wainberg, M.A., and Liang, C. (2016). CRISPR/Cas9-Derived Mutations Both Inhibit HIV-1 Replication and Accelerate Viral Escape. Cell Rep. *15*, 481–489. https://doi.org/10.1016/j.celrep.2016.03.042.

19. Samaniego, L.A., Wu, N., and DeLuca, N.A. (1997). The herpes simplex virus immediate-early protein ICP0 affects transcription from the viral genome and infected-cell survival in the absence of ICP4 and ICP27. J. Virol. *71*, 4614–4625. https://doi.org/10.1128/JVI.71.6.4614-4625.1997.

20. Sandri-Goldin, R.M. (2008). The many roles of the regulatory protein ICP27 during herpes simplex virus infection. Front. Biosci. *13*, 5241–5256. https://doi.org/10.2741/3078.

21. Schang, L.M., Hu, M., Cortes, E.F., and Sun, K. (2021). Chromatin-mediated epigenetic regulation of HSV-1 transcription as a potential target in antiviral therapy. Antiviral Res. *192*, 105103. https://doi.org/10.1016/j.antiviral.2021.105103.

22. Weiss, T., Crisp, P.A., Rai, K.M., Song, M., Springer, N.M., and Zhang, F. (2022). Epigenetic features drastically impact CRISPR-Cas9 efficacy in plants. Plant Physiol. *190*, 1153–1164. https://doi.org/10.1093/plphys/kiac285.

23. Bae, S., Park, J., and Kim, J.S. (2014). Cas-OFFinder: a fast and versatile algorithm that searches for potential off-target sites of Cas9 RNA-guided endonucleases. Bioinformatics *30*, 1473–1475. https://doi.org/10.1093/bioinformatics/btu048.

24. Brunet, E., Simsek, D., Tomishima, M., DeKelver, R., Choi, V.M., Gregory, P., Urnov, F., Weinstock, D.M., and Jasin, M. (2009). Chromosomal translocations induced at specified loci in human stem cells. Proc. Natl. Acad. Sci. USA *106*, 10620–10625. https://doi.org/10.1073/pnas.0902076106.

25. Cho, S.W., Kim, S., Kim, Y., Kweon, J., Kim, H.S., Bae, S., and Kim, J.S. (2014). Analysis of off-target effects of CRISPR/Cas-derived RNA-guided endonucleases and nickases. Genome Res. *24*, 132–141. https://doi.org/10.1101/gr.162339.113.

26. Maddalo, D., Manchado, E., Concepcion, C.P., Bonetti, C., Vidigal, J.A., Han, Y.C., Ogrodowski, P., Crippa, A., Rekhtman, N., de Stanchina, E., et al. (2014). In vivo engineering of oncogenic chromosomal rearrangements with the CRISPR/Cas9 system. Nature *516*, 423–427. https://doi.org/10.1038/nature13902.

27. Tsai, S.Q., Zheng, Z., Nguyen, N.T., Liebers, M., Topkar, V.V., Thapar, V., Wyvekens, N., Khayter, C., Iafrate, A.J., Le, L.P., et al. (2015). GUIDE-seq enables genome-wide profiling of off-target cleavage by CRISPR-Cas nucleases. Nat. Biotechnol. *33*, 187–197. https://doi.org/10.1038/nbt.3117.

28. Webre, J.M., Hill, J.M., Nolan, N.M., Clement, C., McFerrin, H.E., Bhattacharjee, P.S., Hsia, V., Neumann, D.M., Foster, T.P., Lukiw, W.J., and Thompson, H.W. (2012). Rabbit and mouse models of HSV-1 latency, reactivation, and recurrent eye diseases. J. Biomed. Biotechnol. *2012*, 612316. https://doi.org/10.1155/2012/612316.

29. Watson, Z.L., Washington, S.D., Phelan, D.M., Lewin, A.S., Tuli, S.S., Schultz, G.S., Neumann, D.M., and Bloom, D.C. (2018). In Vivo Knockdown of the Herpes Simplex Virus 1 Latency-Associated Transcript Reduces Reactivation from Latency. J. Virol. *92*, e00812-18. https://doi.org/10.1128/JVI.00812-18.

30. Issa, S.S., Shaimardanova, A.A., Solovyeva, V.V., and Rizvanov, A.A. (2023). Various AAV Serotypes and Their Applications in Gene Therapy: An Overview. Cells *12*, 785. https://doi.org/10.3390/cells12050785.

31. Dayton, R.D., Wang, D.B., and Klein, R.L. (2012). The advent of AAV9 expands applications for brain and spinal cord gene delivery. Expert Opin. Biol. Ther. *12*, 757–766. https://doi.org/10.1517/14712598.2012.681463.

32. Nicoll, M.P., Hann, W., Shivkumar, M., Harman, L.E.R., Connor, V., Coleman, H.M., Proença, J.T., and Efstathiou, S. (2016). The HSV-1 Latency-Associated Transcript Functions to Repress Latent Phase Lytic Gene Expression and Suppress Virus Reactivation from Latently Infected Neurons. PLoS Pathog. *12*, e1005539. https://doi.org/10.1371/journal.ppat.1005539.

33. Malik, S., Sah, R., Ahsan, O., Muhammad, K., and Waheed, Y. (2023). Insights into the Novel Therapeutics and Vaccines against Herpes Simplex Virus. Vaccines (Basel) *11*, 325. https://doi.org/10.3390/vaccines11020325.

34. Ying, M., Wang, H., Liu, T., Han, Z., Lin, K., Shi, Q., Zheng, N., Ye, T., Gong, H., and Xu, F. (2023). CLEAR Strategy Inhibited HSV Proliferation Using Viral Vectors Delivered CRISPR-Cas9. Pathogens *12*, 814. https://doi.org/10.3390/pathogens12060814.

35. Schiffer, J.T., Mayer, B.T., Fong, Y., Swan, D.A., and Wald, A. (2014). Herpes simplex virus-2 transmission probability estimates based on quantity of viral shedding. J. R. Soc. Interface *11*, 20140160. https://doi.org/10.1098/rsif.2014.0160.

36. Yang, L., Xu, M., Bhuiyan, S.A., Li, J., Zhao, J., Cohrs, R.J., Susterich, J.T., Signorelli, S., Green, U., Stone, J.R., et al. (2022). Human and mouse trigeminal ganglia cell atlas implicates multiple cell types in migraine. Neuron *110*, 1806–1821.e8. https://doi.org/10.1016/j.neuron.2022.03.003.

37. Ouwendijk, W.J.D., Roychoudhury, P., Cunningham, A.L., Jerome, K.R., Koelle, D.M., Kinchington, P.R., Mohr, I., Wilson, A.C., Verjans, G.G.M.G.M., and Depledge, D.P. (2024). Reanalysis of single-cell RNA sequencing data does not support herpes simplex virus 1 latency in non-neuronal ganglionic cells in mice. J. Virol. *98*, e0185823. https://doi.org/10.1128/jvi.01858-23.

38. Mecklenburg, J., Shein, S.A., Malmir, M., Hovhannisyan, A.H., Weldon, K., Zou, Y., Lai, Z., Jin, Y.F., Ruparel, S., Tumanov, A.V., and Akopian, A.N. (2023). Transcriptional profiles of non-neuronal and immune cells in mouse trigeminal ganglia. Front. Pain Res. *4*, 1274811. https://doi.org/10.3389/fpain.2023.1274811.

39. Thalakoti, S., Patil, V.V., Damodaram, S., Vause, C.V., Langford, L.E., Freeman, S.E., and Durham, P.L. (2007). Neuron-glia signaling in trigeminal ganglion: implications for migraine pathology. Headache *47*, 1008–1025. , discussion 1024-1005. https://doi.org/10.1111/j.1526-4610.2007.00854.x.

40. Gombash, S.E., Cowley, C.J., Fitzgerald, J.A., Hall, J.C.E., Mueller, C., Christofi, F.L., and Foust, K.D. (2014). Intravenous AAV9 efficiently transduces myenteric neurons in neonate and juvenile mice. Front. Mol. Neurosci. *7*, 81. https://doi.org/10.3389/fnmol.2014.00081.

41. Watson, Z.L., Ertel, M.K., Lewin, A.S., Tuli, S.S., Schultz, G.S., Neumann, D.M., and Bloom, D.C. (2016). Adeno-associated Virus Vectors Efficiently Transduce Mouse and Rabbit Sensory Neurons Coinfected with Herpes Simplex Virus 1 following Peripheral Inoculation. J. Virol. *90*, 7894–7901. https://doi.org/10.1128/JVI.01028-16.

42. Washington, S.D., Edenfield, S.I., Lieux, C., Watson, Z.L., Taasan, S.M., Dhummakupt, A., Bloom, D.C., and Neumann, D.M. (2018). Depletion of the Insulator Protein CTCF Results in Herpes Simplex Virus 1 Reactivation In Vivo. J. Virol. *92*, e00173-18. https://doi.org/10.1128/JVI.00173-18.

43. Strang, B.L., and Stow, N.D. (2005). Circularization of the herpes simplex virus type 1 genome upon lytic infection. J. Virol. *79*, 12487–12494. https://doi.org/10.1128/JVI.79.19.12487-12494.2005.

44. Bulcha, J.T., Wang, Y., Ma, H., Tai, P.W.L., and Gao, G. (2021). Viral vector platforms within the gene therapy landscape. Signal Transduct. Target. Ther. *6*, 53. https://doi.org/10.1038/s41392-021-00487-6.

45. Hinderer, C., Katz, N., Buza, E.L., Dyer, C., Goode, T., Bell, P., Richman, L.K., and Wilson, J.M. (2018). Severe Toxicity in Nonhuman Primates and Piglets Following High-Dose Intravenous Administration of an Adeno-Associated Virus Vector Expressing Human SMN. Hum. Gene Ther. *29*, 285–298. https://doi.org/10.1089/hum.2018.015.

46. Morales, L., Gambhir, Y., Bennett, J., and Stedman, H.H. (2020). Broader Implications of Progressive Liver Dysfunction and Lethal Sepsis in Two Boys following Systemic High-Dose AAV. Mol. Ther. *28*, 1753–1755. https://doi.org/10.1016/j.ymthe.2020.07.009.

47. Kishimoto, T.K., and Samulski, R.J. (2022). Addressing high dose AAV toxicity - 'one and done' or 'slower and lower. Expert Opin. Biol. Ther. *22*, 1067–1071. https://doi.org/10.1080/14712598.2022.2060737.

48. Palazzi, X., Pardo, I.D., Sirivelu, M.P., Newman, L., Kumpf, S.W., Qian, J., Franks, T., Lopes, S., Liu, J., Monarski, L., et al. (2022). Biodistribution and Tolerability of AAV-PHP.B-CBh-SMN1 in Wistar Han Rats and Cynomolgus Macaques Reveal Different Toxicologic Profiles. Hum. Gene Ther. *33*, 175–187. https://doi.org/10.1089/hum.2021.116.

49. Schuster, D.J., Dykstra, J.A., Riedl, M.S., Kitto, K.F., Belur, L.R., McIvor, R.S., Elde, R.P., Fairbanks, C.A., and Vulchanova, L. (2014). Biodistribution of adeno-associated virus serotype 9 (AAV9) vector after intrathecal and intravenous delivery in mouse. Front. Neuroanat. *8*, 42. https://doi.org/10.3389/fnana.2014.00042.

50. Mullard, A. (2021). Gene therapy community grapples with toxicity issues, as pipeline matures. Nat. Rev. Drug Discov. *20*, 804–805. https://doi.org/10.1038/d41573-021-00164-x.

51. Hanlon, K.S., Kleinstiver, B.P., Garcia, S.P., Zaborowski, M.P., Volak, A., Spirig, S.E., Muller, A., Sousa, A.A., Tsai, S.Q., Bengtsson, N.E., et al. (2019). High levels of AAV vector integration into CRISPR-induced DNA breaks. Nat. Commun. *10*, 4439. https://doi.org/10.1038/s41467-019-12449-2.

52. Wu, H., Zhang, S., Qiu, W., Zhang, G., Xia, Q., Xiao, C., Huang, X., Huang, M., Agen, P., Fan, T., et al. (2001). Isolation, characterization, and mapping of a novel human KRAB zinc finger protein encoding gene ZNF463. Biochim. Biophys. Acta *1518*, 190–193. https://doi.org/10.1016/s0167-4781(01)00172-5.

53. Jiang, S., Linghu, E., Zhan, Q., Han, W., and Guo, M. (2015). Methylation of ZNF331 Promotes Cell Invasion and Migration in Human Esophageal Cancer. Curr. Protein Pept. Sci. *16*, 322–328. https://doi.org/10.2174/1389203716041504291552555.

54. Wang, Y., He, T., Herman, J.G., Linghu, E., Yang, Y., Fuks, F., Zhou, F., Song, L., and Guo, M. (2018). Correction to: Methylation of ZNF331 is an independent prognostic marker of colorectal cancer and promotes colorectal cancer growth. Clin. Epigenetics *10*, 36. https://doi.org/10.1186/s13148-018-0467-2.

55. Kim, D., Luk, K., Wolfe, S.A., and Kim, J.S. (2019). Evaluating and Enhancing Target Specificity of Gene-Editing Nucleases and Deaminases. Annu. Rev. Biochem. *88*, 191–220. https://doi.org/10.1146/annurev-biochem-013118-111730.

56. Rabinowitz, R., and Offen, D. (2021). Single-Base Resolution: Increasing the Specificity of the CRISPR-Cas System in Gene Editing. Mol. Ther. *29*, 937–948. https://doi.org/10.1016/j.ymthe.2020.11.009.

57. Huang, X., Yang, D., Zhang, J., Xu, J., and Chen, Y.E. (2022). Recent Advances in Improving Gene-Editing Specificity through CRISPR-Cas9 Nuclease Engineering. Cells *11*, 2186. https://doi.org/10.3390/cells11142186.

58. Aubert, M., Boyle, N.M., Stone, D., Stensland, L., Huang, M.L., Magaret, A.S., Galetto, R., Rawlings, D.J., Scharenberg, A.M., and Jerome, K.R. (2014). In vitro Inactivation of Latent HSV by Targeted Mutagenesis Using an HSV-specific Homing Endonuclease. Mol. Ther. Nucleic Acids *3*, e146. https://doi.org/10.1038/mtna.2013.75.

59. Clement, K., Rees, H., Canver, M.C., Gehrke, J.M., Farouni, R., Hsu, J.Y., Cole, M.A., Liu, D.R., Joung, J.K., Bauer, D.E., and Pinello, L. (2019). CRISPResso2 provides accurate and rapid genome editing sequence analysis. Nat. Biotechnol. *37*, 224–226. https://doi.org/10.1038/s41587-019-0032-3.